Mammalian *MagT1* and *TUSC3* are required for cellular magnesium uptake and vertebrate embryonic development

Hao Zhou and David E. Clapham[1]

Department of Cardiology, Howard Hughes Medical Institute, Manton Center for Orphan Disease, Children's Hospital Boston, and Department of Neurobiology, Harvard Medical School, 1309 Enders, 320 Longwood Avenue, Boston, MA 02115

Contributed by David E. Clapham, July 26, 2009 (sent for review July 7, 2009)

Magnesium (Mg^{2+}) is the second most abundant cation in cells, yet relatively few mechanisms have been identified that regulate cellular levels of this ion. The most clearly identified Mg^{2+} transporters are in bacteria and yeast. Here, we use a yeast complementary screen to identify two mammalian genes, *MagT1* and *TUSC3*, as major mechanisms of Mg^{2+} influx. *MagT1* is universally expressed in all human tissues and its expression level is up-regulated in low extracellular Mg^{2+}. Knockdown of either MagT1 or TUSC3 protein significantly lowers the total and free intracellular Mg^{2+} concentrations in mammalian cell lines. Morpholino knockdown of MagT1 and TUSC3 protein expression in zebrafish embryos results in early developmental arrest; excess Mg^{2+} or supplementation with mammalian mRNAs can rescue the effects. We conclude that *MagT1* and *TUSC3* are indispensable members of the vertebrate plasma membrane Mg^{2+} transport system.

ALR1 | transporter | TRPM | zebrafish | KMG104-AM

Magnesium (Mg^{2+}) is the most abundant divalent cation in eukaryotic cells. Estimates of total intracellular Mg^{2+} concentrations ($[Mg^{2+}]$) vary from 17 to 20 mM in different mammalian cells (1), while free $[Mg^{2+}]$ is ≈0.5–1 mM (2–5). The majority of Mg^{2+} is bound to the major building blocks of the cell, such as proteins, phospholipids, nucleic acids, and especially ATP (6). Serum $[Mg^{2+}]$ is maintained in a relatively narrow range (1–2 mM) in mammals (7), only slightly higher than the intracellular free $[Mg^{2+}]$, making the reversal potential for Mg^{2+} close to zero. Thus, the electrochemical gradient for Mg^{2+} is normally into the cell due to the negative plasma membrane potential. Compared to $[Ca^{2+}]$, free $[Mg^{2+}]$ in the cytosol fluctuates much less dramatically with extracellular stimuli (8). Nevertheless, Mg^{2+} plays a fundamentally important role in cellular processes. Mg^{2+} serves as a major cofactor of ATP; >90% of cellular ATP is Mg-ATP (9). Therefore, it is not surprising that cell metabolism and many enzymatic activities are affected by Mg^{2+} homeostasis (10). Mg^{2+} deficiency results in small cell size and cell cycle arrest (11), as well as accelerated cell senescence (12), and intracellular Mg^{2+} levels modulate the activity of many ion channels (13–18). In whole animals, hypomagnesemia results in hypocalcemia (19, 20), and Mg^{2+} deficiency has been correlated to hypertension (21, 22).

Magnesium bond angles for ligand coordination are tightly constrained and Mg^{2+} is almost always hexacoordinated (23). Mg^{2+} binds tightly to H_2O, with very high energies (40–80 kcal/mol) required for dehydration (24, 25). These features dictate that Mg^{2+} transporters should differ in significant ways from other cationic ion channels and transporters. The recently solved structures of bacterial *CorA* (26–28) and *MgtE* (29) Mg^{2+} channels show little overall structural similarity to other cation channels. Interestingly, the *ALR1* gene from *Saccharomyces cerevisiae* shares minimal sequence homology with *CorA*, yet *ALR1* and *CorA* are functionally interchangeable (30, 31).

Recently several vertebrate genes were implicated in Mg^{2+} homeostasis (32). *SLC41A1* (33, 34) and *SLC41A2* (35) genes are remote homologs to the widely expressed prokaryotic Mg^{2+} transporter *MgtE*, and their overexpression in mammalian and avian cells increases total cellular $[Mg^{2+}]$. *SLC41A1* (36), *SLC41A2* (37), *MagT1* (38), *NIPA1* (39), *NIPA2* (40), and *HIP14* (41) have all been proposed to conduct Mg^{2+} currents when overexpressed in *Xenopus* oocytes. Magnesium permeation of several transient receptor potential (TRP) ion channels, such as *TRPM6* (42–44) and *TRPM7* (45, 46), has raised interest in putative Mg^{2+} channels. *TRPM6* mutations have been linked to the human genetic disease familial hypomagnesemia with secondary hypocalcemia (47, 48). *TRPM7* knockout in DT-40 avian lymphocytes exhibited a Mg^{2+} deficiency phenotype and growth arrest (49). However, detailed studies of $[Mg^{2+}]$ in tissues of $TRPM7^{-/-}$ mice show that these channels play little direct role in Mg^{2+} homeostasis (50). The extremely low inward conductance of the TRPM6/7 channels rather suggests that the affects of permeant Mg^{2+} are confined to the immediate vicinity of the channel.

In this report, we took advantage of the growth arrest phenotype of the *S. cerevisiae* Mg^{2+} transporter mutant *alr1*Δ, and performed a complementary screen to search for potential human genes that could rescue the phenotype. We found that *MagT1*, and its homolog, *TUSC3*, support the growth of *alr1*Δ yeast without Mg^{2+} supplementation. We show that both genes are required for mammalian cellular Mg^{2+} uptake and are crucial for zebrafish embryonic development.

Results

***MagT1 and TUSC3* Complement the Yeast *ALR1* Mg^{2+} Transporter.** Growth of yeast *Saccharomyces cerevisiae* strain *alr1*Δ (30, 31) arrests on common YPD medium, and it only proliferates when the media is supplemented with 50–100 mM $MgCl_2$ (Fig. 1*A*). To identify human genes that might complement this defect, we transformed a Jurkat cell library in the yeast *GAL1* expression vector (pNV7-Jurkat) into *alr1*Δ, and collected clones that could grow on normal YPGal medium without Mg^{2+} supplementation. One of the complementation clones contained the sequence from *MagT1* (GeneBank CAB66571.1), encoding a membrane protein with four predicted transmembrane (TM) helices (Fig. 1*B*). *MagT1* was previously identified in an oligonucleotide microarray screen for genes up-regulated in mouse kidney distal convoluted tubule cells under low Mg^{2+} growth conditions (38). *MagT1*'s sequence reveals no similarity to any known bacterial, yeast, or mammalian Mg^{2+} transport genes, except for remote

Author contributions: H.Z. and D.E.C. designed research; H.Z. performed research; H.Z. contributed new reagents/analytic tools; H.Z. and D.E.C. analyzed data; and H.Z. and D.E.C. wrote the paper.

The authors declare no conflict of interest.

Freely available online through the PNAS open access option.

[1]To whom correspondence should be addressed. E-mail: dclapham@enders.tch.harvard.edu.

This article contains supporting information online at www.pnas.org/cgi/content/full/0908332106/DCSupplemental.

www.pnas.org/cgi/doi/10.1073/pnas.0908332106

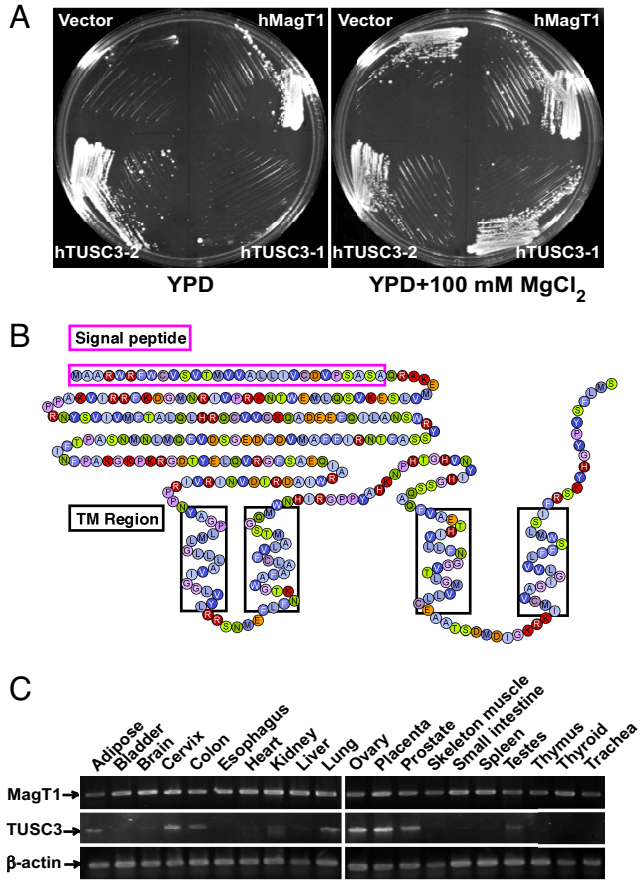

Fig. 1. *MagT1* and *TUSC3* complement the yeast *ALR1* Mg^{2+} transporter-deficient strain. (*A*) Yeast complementation assay. *MagT1* and two splicing isoforms of *TUSC3* were subcloned into the yeast p413GPD expression vector and the *alr1*Δ strain transformed. Yeasts were streaked on either YPD or YPD plates supplemented with 100 mM $MgCl_2$, and grown for 2 days at 30 °C. (*B*) Predicted MagT1 secondary structure with the positions of transmembrane (TM) helices and signal peptide indicated. (*C*) RT-PCR of mRNA from human tissues as indicated.

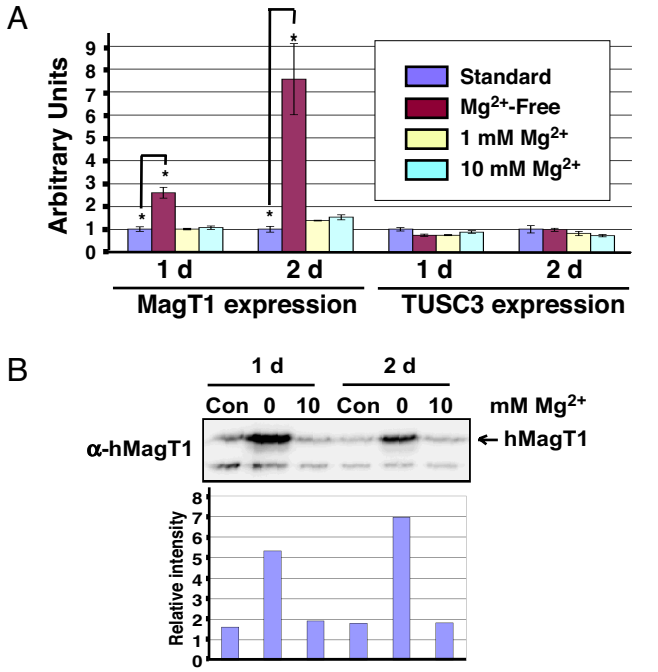

Fig. 2. *MagT1* is up-regulated in low Mg^{2+}. (*A*) Quantitative RT-PCR of total RNA from HEK 293T cells grown in either standard DMEM, or media with the indicated [Mg^{2+}] for 1 or 2 days. Samples were measured in triplicate, and β-actin levels were used as internal controls. Error bars indicate SEM, and asterisks indicate $P < 0.01$. (*B*) Western blots on cells grown in the media indicated in (*A*) using polyclonal antibody against human MagT1. The relative intensity of the Western signal is shown (*Bottom*).

homology to *OST3*, a regulatory subunit of the *S. cerevisiae* endoplasmic reticulum oligosaccharyltransferase complex (51). No clearly defined domains or signature sequences were found in *MagT1*. The predicted topology of MagT1 protein is the inverse of both CorA and MgtE, with a large N-terminal extracellular domain and very small numbers of intracellular residues (Fig. 1*B*). *MagT1* has a human gene homolog, *TUSC3* (GeneBank AAH10370.1), identified as a putative tumor suppressor gene in prostate cancer (Fig. S1) (52). Recently, *TUSC3* has also been found to be associated with autosomal recessive mental retardation (53). *MagT1* and *TUSC3* share 66% identity in the amino acid sequences, with similarly predicted secondary structures, and both are well conserved in mouse, rat, chicken, *Xenopus*, and zebrafish (Fig. S2). In *Drosophila*, only one potential gene, CG7830, is homologous to *MagT1* and *TUSC3*.

We cloned *MagT1* and *TUSC3* into the yeast expression vector p413GPD (54), and verified that either can complement the yeast Mg^{2+} transporter *ALR1* (Fig. 1*A*). *TUSC3* has two predicted splicing variants that differ at their C-termini (Fig. S3). Interestingly, only *TUSC3–2* complemented *ALR1* (Fig. 1*A*). Both *MagT1* and *TUSC3* have four TM domains, and a N-terminal signal peptide predicted to be cleaved from the mature protein (http://www.cbs.dtu.dk/services/SignalP/) (Fig. 1*B*). Cleavage of the N-termini was confirmed by Western blots with tagged proteins. *MagT1* appears to be universally expressed in human; *TUSC3* has a more limited expression pattern, with highest expression in ovary, placenta, prostate, testis, adipose tissue, and lung (Fig. 1*C*). mRNAs of both *MagT1* and *TUSC3* were represented in extracts from HEK-293T (Fig. 2*A*) and Jurkat cell lines.

Extracellular Mg^{2+} Regulates Expression of MagT1. To test the hypothesis that *MagT1* and *TUSC3* are involved in Mg^{2+} transport, we first determined whether *MagT1* expression changes with extracellular [Mg^{2+}]. As shown in Fig. 2*A*, *MagT1* mRNA levels cells increased ≈2.5-fold after 1 day, and 7.5-fold after 2 days of low [Mg^{2+}], while high [Mg^{2+}] incubation had no effect. Meanwhile, *TUSC3* expression was unchanged by either high or low extracellular [Mg^{2+}]. We developed a specific polyclonal antibody against the N-terminal region of human *MagT1* (Fig. S4); Western blots showed similar regulation of MagT1 protein levels in HEK-293T cells (Fig. 2*B*).

MagT1 Is a Cell Surface Protein. Cell surface biotinylation (55) was used to investigate the subcellular localization of MagT1(Fig. 3). Both transfected HA-tagged MagT1 (Fig. 3*A*) and native MagT1 (Fig. 3*B*) were biotinylated in nonpermeabilized HEK 293T cells, indicating that a portion of the total protein was at the cell surface. Upon antibody staining of nonpermeabilized cells with extracellular antibody, only N-terminal-tagged MagT1 was labeled. No signal was detected when the tag was inserted into the loop between putative TM3 and TM4 (see Fig. 1*B*). In contrast, both tags were labeled when the cells were first permeabilized (Fig. 3*C*). These results confirm that MagT1 is at the plasma membrane, but also show that the N terminus of MagT1 is extracellular. The loop between TM1 and TM2, as well as, between TM3 and TM4 would then be intracellular, consistent

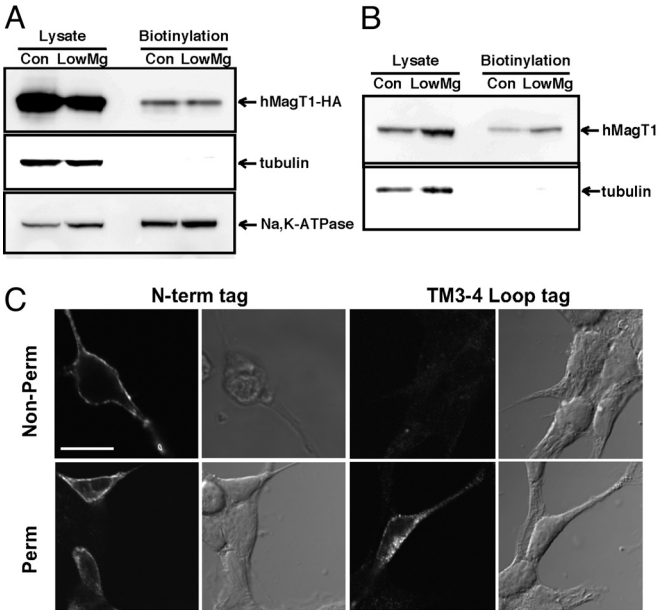

Fig. 3. MagT1 is located on the cell surface. (*A*) Biotinylation of overexpressed MagT1 protein. HEK 293T cells were transfected with HA-tagged *MagT1*, grown for 24 h, and surface proteins labeled by biotinylation. Total cell lysate and streptavidin-purified portions were loaded onto SDS/PAGE gels, and Western blots were performed with α-HA, α-tubulin, or α-Na, K-ATPase antibodies. (*B*) Biotinylation of native MagT1 protein in untransfected HEK 293T cells; native MagT1 protein was detected by α-MagT1 polyclonal antibody. (*C*) Immunostaining of transfected MagT1-HA protein in HEK 293T cells. Permeabilized (0.2% Triton X-100), or nonpermeabilized cell immunostaining with α-HA antibody are compared. (Scale bar, 10 μm.)

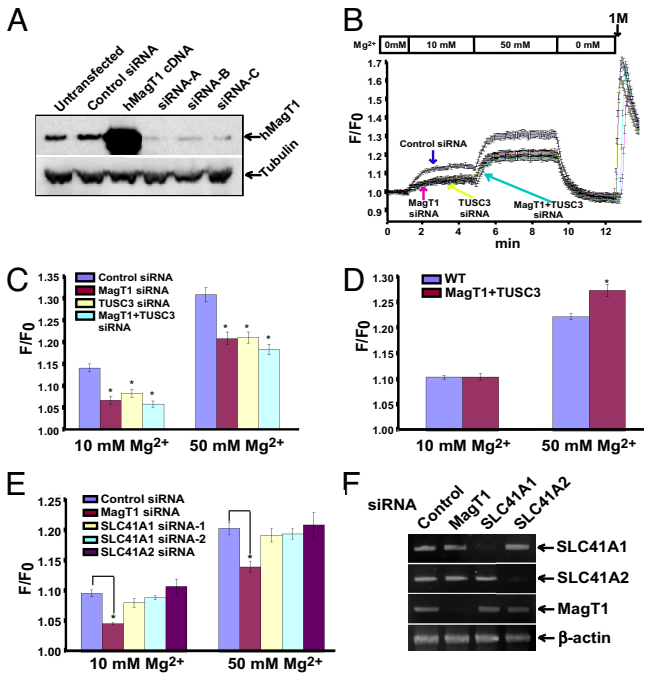

Fig. 4. *MagT1* and *TUSC3* are required for cellular Mg^{2+} uptake. (*A*) RNA interference and overexpression of *MagT1*. HEK 293T cells were transfected with three different siRNAs or *MagT1* cDNA and grown for 2 days before Western blotting total cell lysates using polyclonal α-hMagT1 and α-tubulin antibodies. (*B*) Representative traces of the Mg^{2+} assay in MagT1 knockdown cells. HEK 293T cells were loaded with 20 μM KMG104-AM (45 min, 37 °C), and fluorescence changes monitored in differing [Mg^{2+}]. One molar Mg^{2+} was added at the end of the experiment. (*C*) Quantification of traces in (*B*), with peak fluorescence levels shown for each [Mg^{2+}] treatment; error bars indicate SEM; asterisks indicate $P < 0.01$. (*D*) Mg^{2+} uptake assay on *MagT1* and *TUSC3* overexpressing cells. HEK 293T cells were cotransfected with *MagT1* and *TUSC3* and incubated for 24 h before the assay. (*E*) Mg^{2+} uptake assay in Jurkat cells with potential Mg^{2+} transporters (MagT1, SLC41A1, SLC41A2) knocked down. Each of the indicated siRNAs was transfected into Jurkat cells via electroporation and cells were incubated for 2 days before the assay. (*F*) RT-PCR on total RNA from the Jurkat cells in (*E*).

with the topology predicted by the TMHMM (http://www.cbs.dtu.dk/services/TMHMM-2.0/).

***MagT1* and *TUSC3* Are Required for Mg^{2+} Uptake.** To determine whether MagT1/TUSC3 transport Mg^{2+}, cells were loaded with Mg^{2+}-sensitive dyes and monitored for changes in fluorescence. The cell permeable dye, KMG104-AM (50, 56), has ≈100 times lower affinity for Ca^{2+} than commonly used Mag-Fura2 (57). To reduce MagT1 and TUSC3 protein, we applied small interfering RNA (siRNA) in HEK 293T cells. As shown in Fig. 4*A*, each of the three siRNAs dramatically reduced MagT1 protein levels. *MagT1* and *TUSC3* knockdowns were also verified by RT-PCR from total cell mRNA.

KMG104-AM-loaded HEK 293T cells exhibited a rapid fluorescence increase after the media was switched from a nominally Mg^{2+} free extracellular solution to one containing 10 mM Mg^{2+}. A plateau in the fluorescence signal was reached within approximately 1 min. Upon perfusion with a solution containing 50 mM Mg^{2+}, fluorescence increased further, and returned to baseline when the perfusate was switched back to Mg^{2+} free solution (Fig. 4*B*). In HEK 293T cells treated with control siRNA, free cellular [Mg^{2+}] increased ≈15% upon 10 mM Mg^{2+} application, and ≈30% with 50 mM Mg^{2+} (Fig. 4*C*). MagT1 siRNA-treated cells showed a significantly reduced free $\Delta[Mg^{2+}]$, ≈50–60% of the level in control siRNA-treated cells (Fig. 4 *B* and *C*). Similar effects were observed with TUSC3 siRNA and double (MagT1 and TUSC3) siRNA treatments (Fig. 4 *B* and *C*), indicating that both *MagT1* and *TUSC3* are required for Mg^{2+} uptake.

We overexpressed both *MagT1* and *TUSC3* in HEK 293T cells and measured the change in Mg^{2+} uptake. Although MagT1 (Fig. 4*A*) and TUSC3 levels were significantly increased in the cells upon overexpression, we did not observe a significant difference in $\Delta[Mg^{2+}]$ in 10 mM extracellular [Mg^{2+}], and only a 20% difference in $\Delta[Mg^{2+}]$ in 50 mM extracellular [Mg^{2+}] between mock-transfected and overexpressing cells (Fig. 4*D*).

We monitored total cellular magnesium in HEK cells by Inductively Coupled Plasma Mass Spectrometry (ICP-MS), an accurate and sensitive measurement of elemental content (58). HEK 293T cells were grown in low Mg^{2+} media overnight before they were transferred to media containing normal [Mg^{2+}] (2 mM). Compared to control cells, cells treated with MagT1 siRNA showed significantly lower total Mg^{2+} content, both in standard and low Mg^{2+} media, and slower cellular Mg^{2+} recovery rates when cells were switched back to standard Mg^{2+} media after Mg^{2+} starvation (Fig. S5*A*). Interestingly, overexpressing *MagT1* alone did not raise the total cellular Mg^{2+} content, while expression of both *MagT1* and *TUSC3* resulted in modestly higher cellular Mg^{2+} content. This difference was especially apparent when cells were first starved of Mg^{2+} and later switched back to Mg^{2+}-rich media (Fig. S5*A*). Calcium content could not be compared using ICP-MS due to technical limitations, but zinc, copper, iron, and manganese levels were not significantly different between MagT1 siRNA-treated cells and control cells (Fig. S5*B*; nickel and cobalt levels were too low to be accurately measured).

We examined net currents resulting from overexpression of *MagT1* and *TUSC3* in HEK 293T cells. No significant difference

was detected with whole cell patch clamp methods in transiently transfected cells or inducible stable cell lines. This contrasts with a reported Mg^{2+}-permeant inward current in *MagT1* mRNA-injected *Xenopus* oocytes (38).

***MagT1/TUSC3* Are Mg^{2+} Transporters in Jurkat Cells.** The bacterial *MgtE* homologs, *SLC41A1* and *SLC41A2*, were reported to function as Mg^{2+} exporters and importers, respectively, in vertebrates (33, 35). In Jurkat cells, which express *SLC41A1*, *SLC41A2* (34), *MagT1* and *TUSC3*, knockdown of *SLC41A1* and *SLC41A2* (Fig. 4*F*) did not reduce or increase Mg^{2+} uptake, while *MagT1* knockdown achieved similar effects as its knockdown in HEK 293T cells (Fig. 4*E*). We conclude that *SLC41A1* and *SLC41A2* do not transport significant amounts of Mg^{2+} in Jurkat cells in comparison to *MagT1* and *TUSC3*, under our conditions.

***MagT1* and *TUSC3* Are Crucial for Zebrafish Embryonic Development.** We used zebrafish (*Danio rerio*) to examine the role of *MagT1* and *TUSC3* in vertebrate embryonic development since *MagT1* and *TUSC3* genes are 80% and 93% identical to their human homologs, respectively. A genome-wide mRNA expression study showed that both are widely distributed in tissues throughout all stages of embryonic development (59).

We designed two sets of morpholinos (60) against both *MagT1* and *TUSC3*, targeting the translation start sites (Morpholino A) and intron-exon borders (Morpholino B). By blocking translation initiation, Morpholino A reduces both maternal and zygotic protein levels; Morpholino B interferes with mRNA splicing and only affects zygotic expression. Thirty hours after injection, MagT1 protein levels in the embryos injected with Morpholino A were reduced to <10% of those in the mock injections, and Morpholino B injection resulted in a 78% protein reduction of MagT1 (Fig. 5*A*). Morpholino B dramatically blocked mRNA splicing of *MagT1* (Fig. 5*B*).

We compared the hatching rate of morpholino-injected embryos to that of mock-injected counterparts after 48 h. The injection of MagT1 Morpholino A alone abrogated embryos procession to hatch; TUSC3 Morpholino A decreased hatching rates to ≈30% (Fig. 5*C*). MagT1 or TUSC3 Morpholino B injected embryos had comparable hatching rates as mock-injected controls (≈90%; Fig. 5*C*), perhaps as a result of residual protein expression from maternal mRNA translation. However, when combined Morpholino B oligos against *MagT1* and *TUSC3* were injected, only 20% of the embryos hatched (Fig. 5*D*). These results indicate that both *MagT1* and *TUSC3* are important for zebrafish embryonic development and function cooperatively. Profound developmental abnormalities were apparent 30 h after injection with combined Morpholino A oligos against *MagT1* and *TUSC3* (Fig. 5*E*) as only 5% of the embryos hatched (Fig. 5*D*).

We next determined whether the observed embryonic developmental arrest was correlated with Mg^{2+} deficiency secondary to MagT1/TUSC3 ablation. When human *MagT1* and *TUSC3* mRNA was coinjected with combined MagT1 and TUSC3 Morpholino A (Fig. 5*A*, Lane 3), the hatching rate was increased 4-fold, to 25%. When 10 mM $MgCl_2$ was included in the Morpholino A injection buffer, a 22% survival rate was achieved (Fig. 5*D*). Either *hMagT1+TUSC3* mRNA coinjection with morpholino B, or Mg^{2+} coinjection with Morpholino B, also partially rescued the phenotype (Fig. 5*D*).

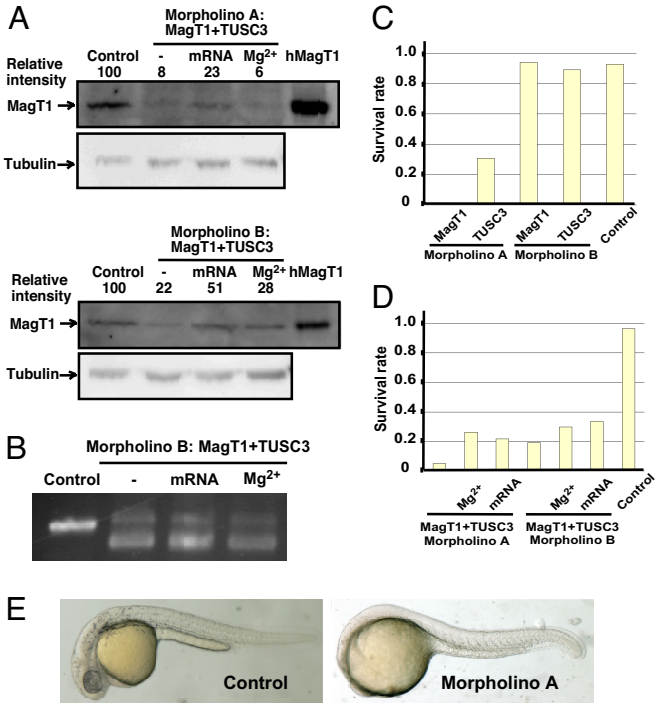

Fig. 5. *MagT1* and *TUSC3* are required for zebrafish embryonic development. (*A*) Western blots of zebrafish embryo total lysates. Fertilized eggs were injected by one of two combinations of morpholinos against both *MagT1* and *TUSC3* (Morpholino A, Morpholino B; 100 μM each in final concentration) or buffer alone (Control). Embryos were collected after 30 h, homogenized, lysed, and anti-MagT1 and -tubulin antibodies used to recognize zebrafish proteins. Lysate from HEK cells with stable MagT1 expression (hMagT1) served as control. Sets of the same eggs were also coinjected with either 100 ng/μL of human *MagT1* and *TUSC3* mRNA, or 10 mM $MgCl_2$, as indicated. The ratio between the MagT1 and tubulin signals was calculated and normalized to the controls. (*B*) RT-PCR of total RNA from the embryos injected with Morpholino B, showing effects on splicing. Eggs were injected as in (*A*), with the Morpholino B set. (*C*) Embryo survival rates after single morpholino injection. 48 h after injections with 200 μM each of the morpholinos indicated, survival rates were calculated as the ratio between total hatched larvae and total eggs injected. (*D*) Double morpholino injections and rescue by coinjection with Mg^{2+} and human MagT1 and TUSC3 mRNA. Eggs were injected with a combination of morpholinos against *MagT1* and *TUSC3* as in (*A* and *B*), and survival rates were calculated as in *C*. For *C* and *D*, 40–70 embryos were counted for each injection. Control, mock injection with buffer. (*E*) Zebrafish development is arrested after morpholino treatment. Fertilized eggs were injected with a combination of morpholino A against *MagT1* and *TUSC3* (100 μM each in final concentration) or buffer alone. Images: 30 h stage.

Discussion

We showed that *MagT1* and *TUSC3* genes underlie a major component in cellular Mg^{2+} transport and are required for vertebrate embryonic development.

Perhaps due to magnesium's unique chemistry, Mg^{2+} transporters share little similarity with other ion transporters or channels. Different families of purported Mg^{2+} transporters share few common signature domains (32, 61), making it difficult to identify new transporters through homology searches. In this report we designed a functional screen for complementary genes in yeast that did not rely on sequence similarity. *MagT1* shares no sequence homology with any known Mg^{2+} transporters, yet it fully complemented the yeast Mg^{2+} deficiency phenotype.

MagT1 and *TUSC3* share significant similarity, and knockdown of either or both genes similarly reduced Mg^{2+} uptake, suggesting that the two gene products function cooperatively. Interestingly, *MagT1* is more universally expressed than *TUSC3*, raising the possibility that MagT1 may function alone or in conjunction with other proteins. Meanwhile, despite almost complete ablation of cellular MagT1, significant residual Mg^{2+} uptake activity remained, suggesting additional Mg^{2+} transport mechanisms. It is worth noting, however, that while both *SLC41A1* and *SLC41A2* were reported to mediate large currents when expressed in *Xenopus* oocytes (36, 37), no significant Mg^{2+} currents were recorded upon overexpression in mammalian and

avian systems (33, 35). Also, in contrast to the currents reported by Goytain and Quamme in *Xenopus* oocytes (38), we did not record current associated with overexpression of *MagT1* and *TUSC3* in mammalian cells.

Although the reduction of MagT1 and TUSC3 in our cell lines resulted in significantly lower levels of both free and total cellular Mg^{2+}, overexpression of the two genes caused only modest increases in Mg^{2+}. This might be explained if native MagT1 and TUSC3 in these cells have already reached their V_{max}, or the overexpressed protein is not properly inserted into the plasma membrane. Alternatively, it is possible that other unidentified proteins impose rate limiting constraints. Nonetheless, as evidenced by our zebrafish experiments, we conclude that *MagT1* and *TUSC3* each play a central role in vertebrate embryonic development that cannot be compensated by other putative Mg^{2+} transporters. The phenotype could be partially rescued by supplying extra Mg^{2+} to zebrafish embryos.

Cells have robust homeostasis mechanisms to confine intracellular $[Mg^{2+}]$ to within a relatively narrow range (1). Even after 48 h Mg^{2+} starvation, HEK 293T cells maintained ≈90% of their total cellular Mg^{2+} without excessive cell death (Fig. S5*A*). Up-regulation of *MagT1* might compensate for low extracellular $[Mg^{2+}]$, but we currently have little knowledge of potential other compensatory mechanisms, such as decreases in Mg^{2+} efflux, release from intracellular compartments, and changes in protein and ATP binding. Future experiments will be necessary to explore the molecular details of *MagT1*, *TUSC3*, and other proteins that control intracellular Mg^{2+} levels.

Materials and Methods

Screen for Mammalian Mg^{2+} Transporters. *S. cerevisiae alr1*Δ strain JS74B and the human Jurkat cDNA expression library pNV7-Jurkat were gifts from R. Schweyen (University of Vienna, Austria) and D. Thiele (Duke University, NC), respectively. Fifty-five micrograms of library DNA were transformed into JB74B to generate ≈1,100,000 transformants; these were spread on YPGal plates to allow expression and selection for growth without Mg^{2+} supplementation. Fifty-five colonies resulted, and the plasmids were sequenced; among these, three included parts of the *MagT1* gene.

Cloning and Molecular Biology. Whole length cDNA of *MagT1* and *TUSC3* was obtained by RT-PCR from HEK 293T cell mRNA. For overexpression, the cDNA was subcloned into pcDNA3.1. Due to the cleavage of N-terminal signal peptides and unstable C-terminal tagged expression, GFP and HA tags were inserted after the signal peptide between residues 29 and 30 of MagT1 and 41 and 42 of TUSC3, respectively. Tags were also inserted into the TM3–4 loop between residues 290 and 291 of MagT1 and 302 and 303 of TUSC3. The integrity of these tagged proteins was verified by Western blots and their subcellular localization was comparable to untagged proteins in immunostaining experiments. For RT-PCR, total RNA was extracted with TRIzol reagent (Invitrogen) and SuperScript III (Invitrogen) used. For quantitative PCR, reverse-transcribed cDNA from ≈0.05 μg total RNA was used as template with SYBR Green kit (Applied Biosystems) on an Eppendorf Realplex4 Mastercycler. β-actin levels were used as internal controls.

Protein Analysis and Western Blots. Standard Western blot procedures were followed. α-human MagT1 antibody was generated by immunizing rabbits with a synthesized peptide with the N-terminal sequence (INFPAKGKPKRGDTYELQV); 0.2 μg/mL antibody was used for Western analysis. The intensity of the Western signal was quantified with the ImageJ program. Biotinylation was carried out with the Cell Surface Protein Isolation Kit (Pierce #89881).

Cell Culture and siRNA. HEK 293T and Jurkat cells were grown in standard DMEM and RPMI 1640 media, respectively, supplemented with 10% FBS (FBS). Solutions containing nominally 0 mM $[Mg^{2+}]$ are designated as "low Mg^{2+}" solutions. For low Mg^{2+} media, FBS-containing media were incubated in Chelex 100 resin (Bio-Rad) twice before 1 mM $CaCl_2$ was added; pH was adjusted to 7.4. Lipofectamine (Invitrogen) and electroporation (Amaxa Biosystems) methods were used to transfect HEK 293T and Jurkat cells, respectively. siRNA was purchased from Ambion using the Silencer Predesigned siRNA library; 50–250 nM was transfected into cells followed by 2–3 days incubation before use.

ICP-MS and Mg Imaging. For ICP-MS, cells were grown in media with differing $[Mg^{2+}]$ before collection and digestion with 1% HNO_3 (95 °C, 4 h). Triplicate samples were diluted and analyzed by ICP-MS in the Department of Earth and Planetary Sciences at Harvard University. Total potassium was measured as an internal control for Mg^{2+} and other metal element measurements; ratios between metals of interest and K^+ were used for data analysis. For Mg^{2+} imaging, cells were loaded with 20 μM KMG104-AM at 37 °C for 45 min, before wash with extracellular buffer (140 mM NaCl, 3 mM KCl, 1.2 mM KH_2PO_4, 10 mM HEPES, 5 mM glucose, pH 7.4). Solutions based on this buffer with different concentrations of $MgCl_2$ were perfused over cells and fluorescence changes were monitored every 3 s through a 40× objective, and analyzed with MetaFluor software (Molecular Devices). All solutions were adjusted to 300 mOsm/L.

Morpholino Treatment on Zebrafish Embryos. Morpholinos were designed to block the translation initiation (Set A) or intron splicing (Set B) in zebrafish embryos, respectively. The following morpholinos were purchased from Gene Tools: MagT1-A, TAGTTTATGCAACATTTTTGTAGGC; MagT1-B, TTCTTTGTCCATACACTTACCTGCA;TUSC3-A, TGCTCCACCTTCTCTGCCAACATG; TUSC3-B, CGTAAAAGCTATATTTTCACCTGTT. Newly fertilized zebrafish eggs were injected with Morpholino (100 to 200 μM) 48 h before hatch rate was monitored, typically of 40–70 eggs.

ACKNOWLEDGMENTS. We thank Dr. John Mably (Children's Hospital Boston, Harvard Medical School, MA) for advice on the design of zebrafish experiments and for reading the manuscript; Drs. Haoxing Xu, I. Scott Ramsey, and Ingrid Carvacho (Children's Hospital Boston, Harvard Medical School, MA) for electrophysiological experiments; Drs. Zhongxing Chen and Charles Langmuir (Harvard University, MA) for ICP-MS analysis; Dr. Rodulf Schweyen for the *S. cerevisiae alr1*Δ strain; Dr. Dennis Thiele for the pNV7-Jurkat library; Dr. Koji Suzuki (Keio University, Japan) for the KMG-109 a.m. dye; Svetlana Gapon (Children's Hospital Boston, Harvard Medical School, MA) for help on cell culture; and Rachel Reynolds and Michael Sweeney (Children's Hospital Boston, Harvard Medical School, MA) for zebrafish injections.

1. Romani A (2007) Regulation of magnesium homeostasis and transport in mammalian cells. *Arch Biochem Biophys* 458:90–102.
2. Fatholahi M, LaNoue K, Romani A, Scarpa A (2000) Relationship between total and free cellular Mg(2+) during metabolic stimulation of rat cardiac myocytes and perfused hearts. *Arch Biochem Biophys* 374:395–401.
3. Harman AW, Nieminen AL, Lemasters JJ, Herman B (1990) Cytosolic free magnesium, ATP and blebbing during chemical hypoxia in cultured rat hepatocytes. *Biochem Biophys Res Commun* 170:477–483.
4. Raju B, Murphy E, Levy LA, Hall RD, London RE (1989) A fluorescent indicator for measuring cytosolic free magnesium. *Am J Physiol* 256:C540–C548.
5. Tashiro M, Konishi M (1997) Basal intracellular free Mg^{2+} concentration in smooth muscle cells of guinea pig tenia cecum: Intracellular calibration of the fluorescent indicator furaptra. *Biophys J* 73:3358–3370.
6. Romani AM, Maguire ME (2002) Hormonal regulation of Mg^{2+} transport and homeostasis in eukaryotic cells. *Biometals* 15:271–283.
7. Quamme GA (1993) Magnesium homeostasis and renal magnesium handling. *Miner Electrolyte Metab* 19:218–225.
8. Grubbs RD (2002) Intracellular magnesium and magnesium buffering. *Biometals* 15:251–259.
9. Scarpa A, Brinley FJ (1981) In situ measurements of free cytosolic magnesium ions. *Fed Proc* 40:2646–2652.
10. Takaya J, Higashino H, Kobayashi Y (2000) Can magnesium act as a second messenger? Current data on translocation induced by various biologically active substances. *Magnes Res* 13:139–146.
11. Sahni J, Scharenberg AM (2008) TRPM7 ion channels are required for sustained phosphoinositide 3-kinase signaling in lymphocytes. *Cell Metab* 8:84–93.
12. Killilea DW, Ames BN (2008) Magnesium deficiency accelerates cellular senescence in cultured human fibroblasts. *Proc Natl Acad Sci USA* 105:5768–5773.
13. Chuang H, Jan YN, Jan LY (1997) Regulation of IRK3 inward rectifier K^+ channel by m1 acetylcholine receptor and intracellular magnesium. *Cell* 89:1121–1132.
14. Hartzell HC, White RE (1989) Effects of magnesium on inactivation of the voltage-gated calcium current in cardiac myocytes. *J Gen Physiol* 94:745–767.
15. Horie M, Irisawa H, Noma A (1987) Voltage-dependent magnesium block of adenosine-triphosphate-sensitive potassium channel in guinea-pig ventricular cells. *J Physiol* 387:251–272.
16. White RE, Hartzell HC (1988) Effects of intracellular free magnesium on calcium current in isolated cardiac myocytes. *Science* 239:778–780.
17. Shi J, et al. (2002) Mechanism of magnesium activation of calcium-activated potassium channels. *Nature* 418:876–880.
18. Zhang X, Solaro CR, Lingle CJ (2001) Allosteric regulation of BK channel gating by Ca(2+) and Mg(2+) through a nonselective, low affinity divalent cation site. *J Gen Physiol* 118:607–636.

19. Meyer P, Boettger MB (2001) Familial hypomagnesaemia with secondary hypocalcaemia: A new case that indicates autosomal recessive inheritance. *J Inherit Metab Dis* 24:875–876.
20. Shalev H, Phillip M, Galil A, Carmi R, Landau D (1998) Clinical presentation and outcome in primary familial hypomagnesaemia. *Arch Dis Child* 78:127–130.
21. Altura BM, Altura BT, Gebrewold A, Ising H, Gunther T (1984) Magnesium deficiency and hypertension: Correlation between magnesium-deficient diets and microcirculatory changes in situ. *Science* 223:1315–1317.
22. Touyz RM (2008) Transient receptor potential melastatin 6 and 7 channels, magnesium transport, and vascular biology: Implications in hypertension. *Am J Physiol Heart Circ Physiol* 294:H1103–1118.
23. Maguire ME, Cowan JA (2002) Magnesium chemistry and biochemistry. *Biometals* 15:203–210.
24. Blades AT, Jayaweera P, Ikonomou MG, Kebarle P (1990) Studies of alkaline earth and transition metal M^{++} gas phase ion chemistry. *J Chem Phys* 92:5900–5906.
25. Dudev T, Cowan JA, Lim C (1999) Competitive Binding in Magnesium Coordination Chemistry: Water versus Ligands of Biological Interest. *J Am Chem Soc* 121:7665–7673.
26. Eshaghi S, et al. (2006) Crystal structure of a divalent metal ion transporter CorA at 2.9 angstrom resolution. *Science* 313:354–357.
27. Lunin VV, et al. (2006) Crystal structure of the CorA Mg^{2+} transporter. *Nature* 440:833–837.
28. Payandeh J, Pai EF (2006) A structural basis for Mg^{2+} homeostasis and the CorA translocation cycle. *EMBO J* 25:3762–3773.
29. Hattori M, Tanaka Y, Fukai S, Ishitani R, Nureki O (2007) Crystal structure of the MgtE Mg^{2+} transporter. *Nature* 448:1072–1075.
30. Graschopf A, et al. (2001) The yeast plasma membrane protein Alr1 controls Mg^{2+} homeostasis and is subject to Mg^{2+}-dependent control of its synthesis and degradation. *J Biol Chem* 276:16216–16222.
31. MacDiarmid CW, Gardner RC (1998) Overexpression of the Saccharomyces cerevisiae magnesium transport system confers resistance to aluminum ion. *J Biol Chem* 273:1727–1732.
32. Schmitz C, Deason F, Perraud AL (2007) Molecular components of vertebrate Mg^{2+}-homeostasis regulation. *Magnes Res* 20:6–18.
33. Kolisek M, et al. (2008) SLC41A1 is a novel mammalian Mg^{2+} carrier. *J Biol Chem* 283:16235–16247.
34. Wabakken T, Rian E, Kveine M, Aasheim HC (2003) The human solute carrier SLC41A1 belongs to a novel eukaryotic subfamily with homology to prokaryotic MgtE Mg^{2+} transporters. *Biochem Biophys Res Commun* 306:718–724.
35. Sahni J, Nelson B, Scharenberg AM (2007) SLC41A2 encodes a plasma-membrane Mg^{2+} transporter. *Biochem J* 401:505–513.
36. Goytain A, Quamme GA (2005) Functional characterization of human SLC41A1, a Mg^{2+} transporter with similarity to prokaryotic MgtE Mg2+ transporters. *Physiol Genomics* 21:337–342.
37. Goytain A, Quamme GA (2005) Functional characterization of the mouse solute carrier, SLC41A2. *Biochem Biophys Res Commun* 330:701–705.
38. Goytain A, Quamme GA (2005) Identification and characterization of a novel mammalian Mg^{2+} transporter with channel-like properties. *BMC Genomics* 6:48.
39. Goytain A, Hines RM, El-Husseini A, Quamme GA (2007) NIPA1(SPG6), the basis for autosomal dominant form of hereditary spastic paraplegia, encodes a functional Mg^{2+} transporter. *J Biol Chem* 282:8060–8068.
40. Goytain A, Hines RM, Quamme GA (2008) Functional characterization of NIPA2, a selective Mg^{2+} transporter. *Am J Physiol Cell Physiol* 295:C944–C953.
41. Goytain A, Hines RM, Quamme GA (2008) Huntingtin-interacting proteins, HIP14 and HIP14L, mediate dual functions, palmitoyl acyltransferase and Mg^{2+} transport. *J Biol Chem* 283:33365–33374.
42. Chubanov V, et al. (2004) Disruption of TRPM6/TRPM7 complex formation by a mutation in the TRPM6 gene causes hypomagnesemia with secondary hypocalcemia. *Proc Natl Acad Sci USA* 101:2894–2899.
43. Li M, Jiang J, Yue L (2006) Functional characterization of homo- and heteromeric channel kinases TRPM6 and TRPM7. *J Gen Physiol* 127:525–537.
44. Voets T, et al. (2004) TRPM6 forms the Mg^{2+} influx channel involved in intestinal and renal Mg^{2+} absorption. *J Biol Chem* 279:19–25.
45. Nadler MJ, et al. (2001) LTRPC7 is a Mg.ATP-regulated divalent cation channel required for cell viability. *Nature* 411:590–595.
46. Runnels LW, Yue L, Clapham DE (2001) TRP-PLIK, a bifunctional protein with kinase and ion channel activities. *Science* 291:1043–1047.
47. Schlingmann KP, et al. (2005) Novel TRPM6 mutations in 21 families with primary hypomagnesemia and secondary hypocalcemia. *J Am Soc Nephrol* 16:3061–3069.
48. Walder RY, et al. (2002) Mutation of TRPM6 causes familial hypomagnesemia with secondary hypocalcemia. *Nat Genet* 31:171–174.
49. Schmitz C, et al. (2003) Regulation of vertebrate cellular Mg^{2+} homeostasis by TRPM7. *Cell* 114:191–200.
50. Jin J, et al. (2008) Deletion of Trpm7 disrupts embryonic development and thymopoiesis without altering Mg^{2+} homeostasis. *Science* 322:756–760.
51. Knauer R, Lehle L (1999) The oligosaccharyltransferase complex from Saccharomyces cerevisiae. Isolation of the OST6 gene, its synthetic interaction with OST3, and analysis of the native complex. *J Biol Chem* 274:17249–17256.
52. Bashyam MD, et al. (2005) Array-based comparative genomic hybridization identifies localized DNA amplifications and homozygous deletions in pancreatic cancer. *Neoplasia* 7:556–562.
53. Garshasbi M, et al. (2008) A defect in the TUSC3 gene is associated with autosomal recessive mental retardation. *Am J Hum Genet* 82:1158–1164.
54. Mumberg D, Muller R, Funk M (1995) Yeast vectors for the controlled expression of heterologous proteins in different genetic backgrounds. *Gene* 156:119–122.
55. Schuberth HJ, Kroell A, Leibold W (1996) Biotinylation of cell surface MHC molecules: A complementary tool for the study of MHC class II polymorphism in cattle. *J Immunol Methods* 189:89–98.
56. Kubota T, et al. (2004) Investigation of intracellular magnesium mobilization pathways I PC12 cells B simultaneous Mg-Ca fluorescent imaging. *J Am Coll Nutr* 23:742S–744S.
57. Komatsu H, et al. (2004) Design and synthesis of highly sensitive and selective fluorescein-derived magnesium fluorescent probes and application to intracellular 3D Mg^{2+} imaging. *J Am Chem Soc* 126:16353–16360.
58. Woodhouse LR, Abrams SA (2001) *Advances in Isotope Methods for the Analysis of Trace Elements in Man.* (CRC Press, Boca Raton, FL) pp 1–22.
59. Thisse B, et al. (2004) Spatial and temporal expression of the zebrafish genome by large-scale in situ hybridization screening. *Methods Cell Biol* 77:505–519.
60. Summerton JE (2007) Morpholino, siRNA, and S-DNA compared: Impact of structure and mechanism of action on off-target effects and sequence specificity. *Curr Top Med Chem* 7:651–660.
61. Kehres DG, Maguire ME (2002) Structure, properties, and regulation of magnesium transport proteins. *Biometals* 15:261–270.